Materials Advances

ROYAL SOCIETY OF CHEMISTRY

PAPER

View Article Online
View Journal | View Issue

Cite this: *Mater. Adv.*, 2024, 5, 5194

Compatibilization of PLA/PBAT blends with epoxidized canola oil for 3D printing applications†

Mohamed Wahbi, [a] Quintin Litke, [b] David Levin, [b] Song Liu, [b] Kevin J. De France [a] and Marianna Kontopoulou *[a]

Poly(lactic acid) (PLA) is a bioderived and biodegradable thermoplastic biopolyester that is widely used in 3D printing. Although PLA is an excellent example of a high-performance naturally derived building block that has found practical applications in a number of different markets, PLA-printed parts often exhibit poor toughness and brittle mechanical behavior. In order to improve the outlook of PLA in material extrusion (MEX) 3D printing applications, this work aims to develop impact-modified and fully biodegradable blends comprising PLA and poly(butylene adipate-*co*-terephthalate) PBAT, compatibilized with epoxidized canola oil (ECO). Importantly, our approach is fundamentally different from previous examples, which typically rely on non-bioderived or non-biodegradable compatibilizers to improve blend performance. Here, blends of PLA and PBAT having various ratios were prepared by melt compounding with 5 phr ECO. Importantly, the addition of ECO did not significantly alter the rheological properties of the blends, but exerted a plasticizing effect reducing the glass transition and cold crystallization temperatures of the blends. Microstructural and mechanical analyses of compression-molded samples revealed uniform dispersion of PBAT domains within the PLA matrix in the presence of ECO, leading to a 62% and 106% increase in impact strength for blends containing 20 and 30 wt% PBAT, respectively, as compared to non-compatibilized blends. Based on significant improvements in impact strength, 70/30 PLA/PBAT blends with 5 phr ECO were chosen for 3D printing experiments. Parts printed from PLA/PBAT blends displayed poor fusion between strands, resulting in voids and brittle failure during tensile testing. In the case of compatibilized blends, ECO incorporation facilitated fusion between neighboring strands, enhancing ductility during tensile testing. Therefore, we demonstrate that the addition of ECO to PLA/PBAT blends not only enhances compatibilization but also improves printability and strand healing during MEX 3D printing. We anticipate that the results presented here could pave the way for the development of high-performance and fully biodegradable materials and blends through a variety of extrusion-based processing methods.

Received 8th March 2024,
Accepted 5th May 2024

DOI: 10.1039/d4ma00233d

rsc.li/materials-advances

1. Introduction

With increasing regulations surrounding the use of petroleum-based products, thermoplastic biopolyesters have attracted significant attention in recent years because they are biobased and/or biodegradable, and they can be processed using conventional polymer processing equipment.[1,2] At first glance, these materials can therefore serve as plug-and-play replacements to conventional thermoplastics. Unfortunately, most biopolyesters and even more broadly most biopolymers, have largely failed in industrial applications because of their low mechanical properties, insufficient crystallinity, and overall inferior performance.[3] To address these limitations, research has primarily focused on blending such biopolymers in the presence of compatibilizers, plasticizers, and/or reinforcing fillers.[4–6] This strategy is largely scalable, sustainable, and cost-effective, provided that the fully biobased designation can be maintained, and appropriate performance metrics can be demonstrated.[4,7,8]

In nature, composite materials with exceptional mechanical performance are often comprised of both rigid and flexible building blocks. This is apparent, for example, in crustacean shells, composed of rigid chitin nanofibrils bound together by flexible proteins.[9] Learning from nature, researchers have taken a similar approach in the combination of both rigid and elastomeric biopolyesters to create high-performance composites. For example, poly(lactic acid) (PLA; one of the most commonly investigated rigid biopolyesters) has been combined with several different elastomeric biopolyesters such as

[a] *Department of Chemical Engineering, Smith Engineering, Queen's University, Kingston ON, Canada. E-mail: kontopm@queensu.ca*
[b] *Department of Biosystems Engineering, University of Manitoba, Winnipeg, Manitoba, Canada*

† Electronic supplementary information (ESI) available. See DOI: https://doi.org/10.1039/d4ma00233d

medium-chain-length poly(hydroxyl alkanoates) (PHAs), polycaprolactone (PCL), poly(butylene adipate-*co*-terephthalate) (PBAT), and polybutylene succinate (PBS) to enhance blend ductility and toughness.[7,10–12] Among the wide range of elastomeric biopolymer candidates for impact modification, PBAT offers the highest elongation at break (up to 700%) at a reasonable cost.[13,14] It's worth noting that although PBAT is a petroleum-derived copolymer, it is completely biodegradable; it is manufactured using cheap and commercially available monomers, allowing for scalable production.[15]

Several groups have already demonstrated that the incorporation of PBAT into a PLA matrix improves both elongation at break and impact strength, while preserving PLA stiffness.[16–18] Unfortunately, PLA and PBAT demonstrate poor compatibility, which is a significant concern during blending, because of the need for additional interphase compatibilizers to improve the affinity between these two polymers.[19] Several solutions for this problem do exist however, including the use of reactive compatibilizers, low molecular weight (M_W) compatibilizers, catalysts, and block copolymers of PLA and PBAT.[20–22] These strategies allow for enhancing interfacial adhesion and dispersion of the PBAT dispersed phase within the PLA matrix, consequently improving the morphology and enhancing the thermomechanical properties of the blend. Among all such methods, reactive compatibilizers, crosslinking agents, and low M_W additives containing functional groups (*e.g.*, epoxy groups), offer an effective and environmentally friendly strategy for enhancing the compatibility of blends.[4,20,23]

To this end, several reactive compatibilizers have been investigated, including epoxy-functionalized chain extenders (such as Joncryl® ADR series), epoxy-polyhedral oligomeric silsesquioxanes (POSS), dicumyl peroxide (DCP), and epoxidized vegetable oils.[12,17,20,22,24,25] Wang *et al.* reported that adding Joncryl® ADR to PLA/PBAT blends significantly improved the compatibility between the PLA and PBAT phases, consequently increasing both impact strength and elongation at break.[12] Similarly, the incorporation of epoxidized soybean oil (ESO) into the blends was found to enhance compatibility *via* the promotion of polymer branching, leading to significant improvements in elongation at break and impact strength.[17] More recently, it was demonstrated that epoxidized canola oil (ECO) can be an effective and environmentally friendly compatibilizer for PLA/PBAT blends.[23] Here, the incorporation of ECO improved the distribution of PBAT within the PLA matrix, reduced the PBAT dispersed phase size, and improved the interfacial adhesion between PLA and PBAT phases. A composition of 5 phr ECO led to significant improvements in the elongation at break, and good balance in mechanical properties.

Despite the widespread research on PLA/PBAT blends, there are still limited studies on their processing by 3D printing. The necessity for appropriate compatibilization between both phases is largely responsible for this gap in research.[26] Of the few examples that do exist, Lyu *et al.* demonstrated PLA grafted with glycidyl methacrylate (GMA) and showed that the compatibilized blends with PBAT had better interfacial bonding and exhibited ductile fracture.[27] They hypothesized that ductile fracture was observed on the basis of molecular chain entanglement between adjacent printed layers in the presence of the compatibilizer. Andrzejewski *et al.* used PLA and PBAT modified with the multifunctional epoxy-functionalized styrene-acrylic chain extender, Joncryl®, and compared the properties of injection molded and 3D printed samples.[20] They reported that the properties were optimum for the blends containing 30 wt% PBAT and 0.5 phr chain extender. However, this strategy leads to branching and consequently increases the viscosity, thus compromising the extrudability of these blends.[20] Building on such limited results, in this study we aim to develop fully biodegradable or compostable PLA/PBAT blends compatibilized with ECO that are suitable for processing by material extrusion (MEX) 3D printing. Given the widespread popularity of PLA in 3D printing applications, it is still mainly used for the production of prototypes. Having access to impact modified PLA-based blends with good balance of properties, while maintaining biodegradability will advance the state-of-the-art in MEX 3D printing. This work will thus enable the use of PLA-based formulations in high-value-added specialty 3D printed products. We first demonstrate the effectiveness of ECO as a compatibilizer and toughening agent for PLA/PBAT, enabling the uniform distribution of PBAT within the PLA matrix and improving PLA toughness. We then explore the printability of PLA/PBAT/ECO blends; and report the effect of ECO on the quality of the printed parts.

2. Materials and methods

2.1 Materials

Polylactic acid (PLA) Ingeo™ Biopolymer 3001D, injection molding grade (MFR of 22 g/10 min at 210 °C/2.16 kg) was purchased from NatureWorks LLC (Minnesota, USA). Biodegradable poly(butylene adipate-*co*-terephthalate) (PBAT) Ecoflex® F Blend C1200 (MFR of 2.7–4.9 g/10 min at 190 °C/2.16 kg) was provided by BASF (Mississauga, Ontario, Canada). Epoxidized canola oil (ECO) was synthesized in-house using the procedures outlined in our previously published paper.[23] All materials were used as received.

2.2 Preparation of PLA/PBAT blends

Prior to melt-blending, PLA and PBAT pellets were dried under vacuum in a lab oven at 60 °C for 24 hours to eliminate any traces of moisture. PBAT pellets were pre-mixed with PLA at different compositions (80/20, 70/30, and 60/40 PLA/PBAT ratio by weight) before blending. A preheated (190 °C) Haake Polylab torque rheometer connected to a Rheomix R600 batch mixer was utilized to prepare the polymer blends. Non-compatibilized PLA/PBAT blends were prepared by adding the pre-mixed pellets to the chamber and melt-blending for 5 minutes at 100 rpm and 190 °C.

To prepare the ECO compatibilized PLA/PBAT/ECO blends, first the pre-mixed PLA/PBAT pellets were melt-blended for 1 minute at 50 rpm. Then, 5 parts per hundred resin (phr) of ECO was added to the mixture and the rotor speed was increased to 100 rpm until the torque stabilized (approximately 5 minutes). The chemical structures of PLA, PBAT, and ECO

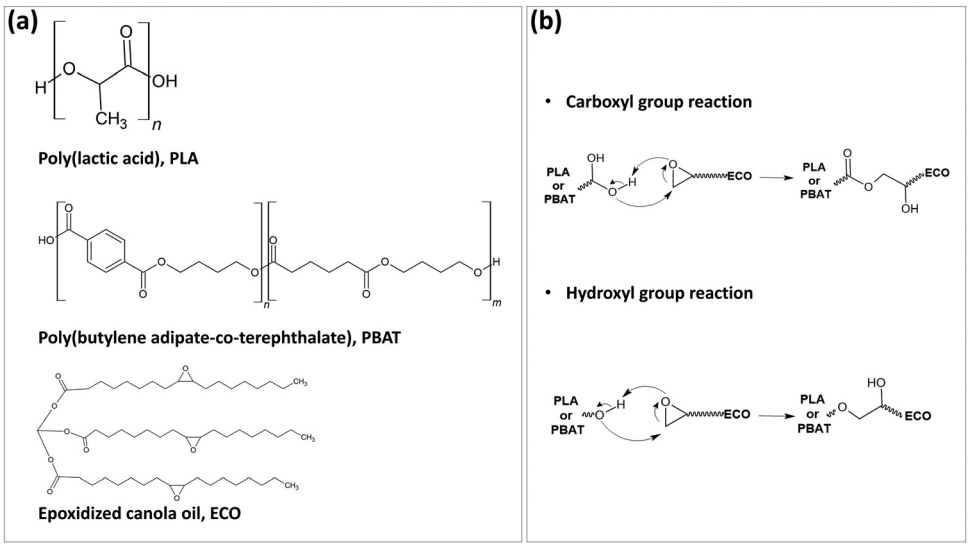

Scheme 1 (a) Chemical structure of PLA, PBAT, and ECO, (b) mechanism of possible reactions between PLA and PBAT with ECO.

along with the mechanisms of possible reactions between PLA and PBAT with ECO are shown in Scheme 1. All blended formulations used in this work are described in Table S1 (ESI†).

2.3 Fabrication of 3D printed specimens

After completing preliminary experiments, as described in Section 3.5, 70/30 blends of PLA/PBAT with and without ECO were used for MEX 3D printing. An Allevi 1 Bioprinter (Allevi Inc, USA) was used to create 3D printed tensile specimens. The printer consists of a core extruder that is connected to an air compressor (Senco, model PC1010) to provide compressed air to the system. A cylindrical pellet feeder and a 0.4 mm diameter printing nozzle at the bottom was used, along with a horizontal metal printing platform.

To print the specimens, the polymer blends were first chopped into small pieces and added to a preheated feeder. Once completely melted at the printing temperature (190 °C), the Allevi Bioprint software was used to initiate the printing process. MEX 3D printed samples were fabricated according to the ASTM D638 type V standard. In this study, we printed dumbbell specimens of 0.2 mm layer high, 0.3 mm interstrand spacing at 0° raster angle (longitudinal direction) and at 20 mm s^{-1} printing speed. The printing conditions are summarized in Table S4 (ESI†).

2.4 Characterizations

The morphology and microstructure of the prepared blends and printed specimens were analyzed using a ThermoFisher Quanta 250 eSEM with a field emission gun and a Gaseous secondary electron detector in a high-pressure chamber. SEM micrographs of compression molded samples were obtained from the Izod notched impact test specimens. The fractured surfaces were palladium-coated under vacuum for 90 seconds to prevent surface charging. For the 3D printed samples, tensile tested specimens were used. The SEM images were analyzed using ImageJ software to estimate the average diameters of the dispersed PBAT phase, as well as to calculate the polydispersity index. Between 60 and 100 PBAT particles were analyzed per sample. The average particle size diameters (D) of the PBAT phase and the polydispersity index (PI) were calculated according to the formulas described elsewhere.[28]

The compatibilization reactions were confirmed using Attenuated total reflectance-Fourier transform infrared (ATR-FTIR) spectroscopy with a diamond ATR crystal using a Nicolet iS10 FTIR Spectrometer (ThermoFisher Scientific Inc., Oakville, ON, Canada). All samples are used as received.

The tensile properties of both 3D-printed and compression-molded samples were measured using a Universal Tester (Instron 3369), in accordance with ASTM D638-5 standards. Compression-molded specimens were prepared by preparing rectangular sheets using a Carver hydraulic press, from which dumbbell shapes were punched out using a QualiTest D635 type 5 cutting die. To ensure consistency, at least five specimens of each sample were tested for both the printed and compression-molded samples. Tensile tests for all samples were carried out at a crosshead speed of 1 mm min^{-1}, with a gauge distance of 25 mm at room temperature.

The Notched Izod impact strength measurements were carried out using an Izod Notched Impact Tester (SATEC System Inc.), following the ASTM D256 standards. For each sample, at least five rectangular bars measuring 3 mm × 12.5 mm × 125 mm were prepared by compression molding and then notched using a motorized cutting machine. The specimens were then tested under ambient conditions. The Izod impact strength was determined by dividing the absorbed energy measured during testing by the thickness of the specimen.

The viscoelastic behavior of PLA/PBAT and PLA/PBAT/ECO blends was investigated by conducting rheological measurements at 190 °C, which corresponds to the compounding and extrusion temperature. Compression molded discs of 25 mm diameter and 1 mm in thickness were used after being dried overnight under vacuum. The rheological tests were performed on an Anton Paar MCR 301 rheometer equipped with a 25 mm

parallel plate at a sample gap of 1 mm and at 190 °C for all samples. To determine the linear viscoelastic region, strain sweeps were carried out from 0.1 to 100% at 1 rad s^{-1}, after which small amplitude oscillatory shear (SAOS) tests were performed with a constant strain amplitude of 5% and a frequency range of 0.1–100 rad s^{-1} for each sample.

The thermal transitions and crystallization behavior of the prepared blends were investigated using differential scanning calorimetry on a DSC Q1000 instrument (TA Instruments, USA). Approximately 5–10 mg of each sample were sealed in aluminum hermetic pans and heated from room temperature to 250 °C at a heating rate of 5 °C min^{-1} under a nitrogen atmosphere. The samples were held at 250 °C for 2 minutes to erase any prior thermal history. The samples were then cooled down to −50 °C at a cooling rate of 5 °C min^{-1} and kept at this temperature for 2 minutes, after which a second heating cycle was performed from −50 °C to 250 °C at a heating rate of 5 °C min^{-1}. The curves from the second heating run presented in Fig. 3 are used to obtain the glass transition temperature (T_g), the melting temperature (T_m), the cold crystallization temperature (T_{cc}), the melting enthalpy (ΔH_m), and the cold crystallization enthalpy (ΔH_c). The degree of crystallinity of PLA was evaluated according to eqn (1):

$$\chi_c = \frac{\Delta H_m - (\Delta H_{c1} + \Delta H_{c2})}{w_{f,PLA}.\Delta H^{\circ}_{m,PLA} + w_{f,PBAT}.\Delta H^{\circ}_{m,PBAT}} \times 100\% \quad (1)$$

where $\Delta H^{\circ}_{m,PLA} = 93.7\ J\ g^{-1}$ and $\Delta H^{\circ}_{m,PBAT} = 114\ J\ g^{-1}$ are the melting enthalpies of 100% crystalline PLA and PBAT, respectively. $w_{f,PLA}$ and $w_{f,PBAT}$ are the weight fractions of PLA and PBAT in the blend.

The thermal stability of the prepared blends was investigated using TGA on a Q500 TGA instrument (TA Instruments, USA). Approximately 10 mg of each sample was heated from room temperature to 700 °C at 10 °C min^{-1} under a nitrogen atmosphere.

3. Results and discussion

3.1 Compatibilization of PLA/PBAT blends in the presence of ECO

The oxirane rings in ECO can react with the terminated carboxyl groups and/or hydroxyl groups of PLA and PBAT, resulting in improved interfacial interactions, and therefore better compatibility between the PLA and PBAT phases. To investigate this mechanism, ATR-FTIR spectroscopy was used to confirm that oxirane rings in ECO have reacted with PLA and PBAT end groups. Scheme 1 shows the mechanisms of the oxirane ring opening reactions with hydroxyl and carboxyl groups. ATR-FTIR spectra of all blends and a zoomed zone (650–950 cm^{-1}) of ECO and a compatibilized sample (80/20/5) are shown in Fig. 1. The peaks at 1740 cm^{-1}, 1742 cm^{-1}, and 1712 cm^{-1} are attributed to the stretching vibration of C═O in ECO, PLA, and PBAT, respectively. The peaks at 1180 cm^{-1} and 1164 cm^{-1} correspond to the O═C–O groups in PLA and PBAT. The peak at 1271 cm^{-1} is attributed to C═C bonds in the benzene ring structure of PBAT. The peak at 825 cm^{-1} is assigned to the oxirane ring in ECO (zoomed spectrum). The disappearance of this oxirane peak is an indication that the ring opening reaction takes place, as shown in the zoomed spectrum of the sample 80/20/5.[17,23] However, contrary to the observations by Han *et al.*, who used epoxidized soybean oil, in the present work we did not observe any gel formation.[17]

3.2 Morphological analysis of the blends

Fig. 2 shows SEM micrographs of impact test fractured surfaces of PLA/PBAT and PLA/PBAT/ECO blends containing 20–40 wt% PBAT. Previous studies have reported that PLA and PBAT are

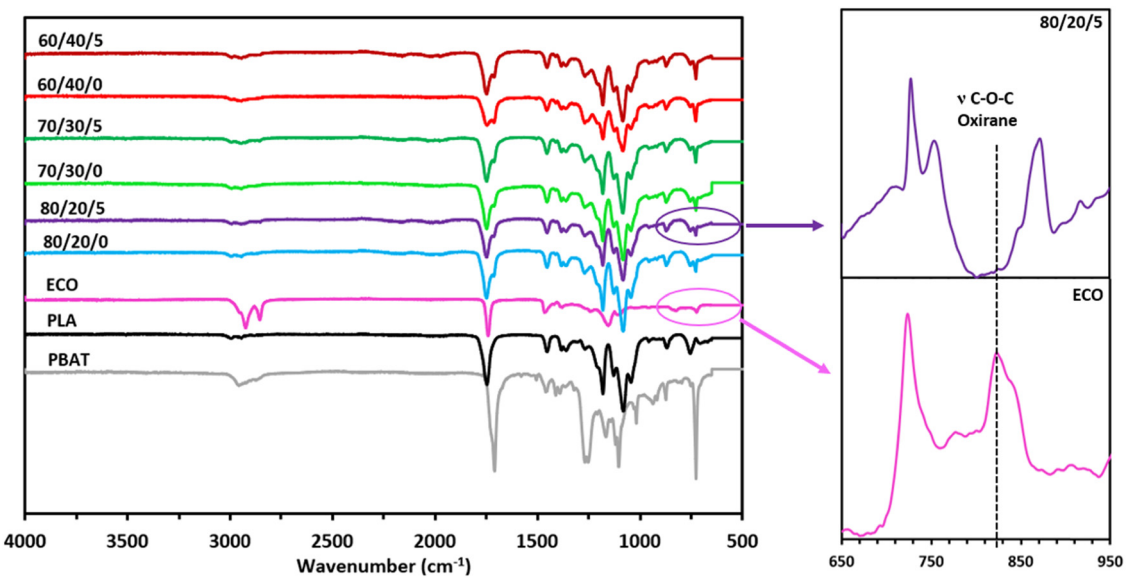

Fig. 1 FTIR spectra of neat polymers, ECO, and all PLA/PBAT blends.

immiscible and exhibit phase separation in most cases.[29,30] However, Deng *et al.* found that PBAT begins to form a co-continuous phase at a critical weight fraction ranging from 19 to 40 wt%, which leads to improved toughness and elongation.[19]

Here the fractured surfaces of non-compatibilized PLA/PBAT blends exhibit droplet matrix morphology (Fig. 2a–c). With an increase in the PBAT content, the size of the droplets becomes larger, from 2.73 ± 0.91 μm for the blend containing 20 wt% PBAT to 4.59 ± 1.08 μm for the blend containing 40 wt% PBAT, and there is clear evidence of debonding of PBAT particles, indicating poor phase interactions (Fig. 2c).

All PLA/PBAT/ECO blends demonstrated a well-dispersed PBAT phase (see Fig. 2d–f). The 80/20/5 and 70/30/5 blends had more uniform particle size when compared to the non-compatibilized PLA/PBAT blends, as demonstrated in Table S2 (ESI†), suggesting that the addition of ECO had a compatibilizing effect on the blends, according to the reactions shown in Scheme 1(b). On the contrary, the 60/40/5 blend showed coarsening of the structure, suggesting that the amount of ECO was not sufficient to achieve a compatibilizing effect.

3.3 Thermal properties of the blends

DSC and TGA analyses were conducted to investigate the thermal behavior and stability of the blends. Table 1 summarizes the thermal transitions and degree of crystallinity recorded from the DSC measurements (2nd heating), while Fig. 3a shows the second heating thermograms of neat PLA, neat PBAT, and all PLA/PBAT blends. The glass transition of PLA exhibited a significant shift with increasing the PBAT concentration, from 58.2 °C for pure PLA to 51.1 °C in the 70/30/0 blend. Similarly, the T_{cc} of PLA showed a notable decline with the increasing PBAT concentration, by 20.8 °C for the 70/30/0 blend. This result indicates the facilitation of the cold crystallization of PLA upon adding PBAT, which is desirable in 3D printing.[29] The lack of crystallization of PLA upon cooling is confirmed by the absence of a crystallization peak of PLA in the DSC exotherm, as shown in Fig. S1 (ESI†). Slow crystallization, characterized by longer cooling times, directly translates to extended printing durations, posing challenges in the utilization of pure PLA in 3D printing.[31] The degree of crystallinity of PLA generally increased with increasing concentration of PBAT in the blend (Table 1), suggesting a nucleating or a plasticizing effect in the presence of the PBAT phase.[23] However, this phenomenon levels off at a composition of 40 wt% PBAT. The degree of crystallinity of the PLA phase was increased from 5.4% for neat PLA to 13.0% for the 70/30/0 blend.

Table 1 Thermal parameters and degree of crystallinity of PLA/PBAT and PLA/PBAT/ECO blends

Sample	T_g (°C)	T_m (°C)	ΔH_m (J g^{-1})	T_{cc1} (°C)	Δ_{c1} (J g^{-1})	T_{cc2} (°C)	Δ_{c2} (J g^{-1})	χ_c (%)
PLA	58.2	167.1	46.5	104.2	41.4	—	—	5.4
PBAT	−32.6	120.8	20.8	—	—	—	—	—
80/20/0	54.2	164.4	34.5	92.9	24.6	147.8	4.2	5.8
80/20/5	54.9	164.3	39.2	86.6	20.9	151.6	1.5	17.2
70/30/0	51.1	163.0	36.5	83.4	21.1	146.7	2.4	13.0
70/30/5	50.3	160.9	33.0	82.2	14.8	—	—	18.2
60/40/0	58.4	165.9	30.5	93.4	20.7	150.8	3.2	6.5
60/40/5	49.2	161.3	28.8	81.6	18.6	148.6	1.1	8.9

It has been reported that epoxidized vegetable oils, such as canola oil, soybean oil, and corn oil, exhibit a plasticizing effect on PLA-based blends, facilitating the mobility of PLA chains and resulting in a significant increase in the crystallinity of the PLA phase.[11,17,32] More importantly, epoxidized vegetable oils act as a compatibilizer for PLA and PBAT blends by increasing the interactions between the two phases. Fig. 3a and Table 1 highlight the effect of adding ECO on the thermal properties of PLA/PBAT blends. While the incorporation of ECO into the PLA/PBAT blends did not lead to significant shifts in the glass transition of PLA, it slightly decreased the cold crystallization

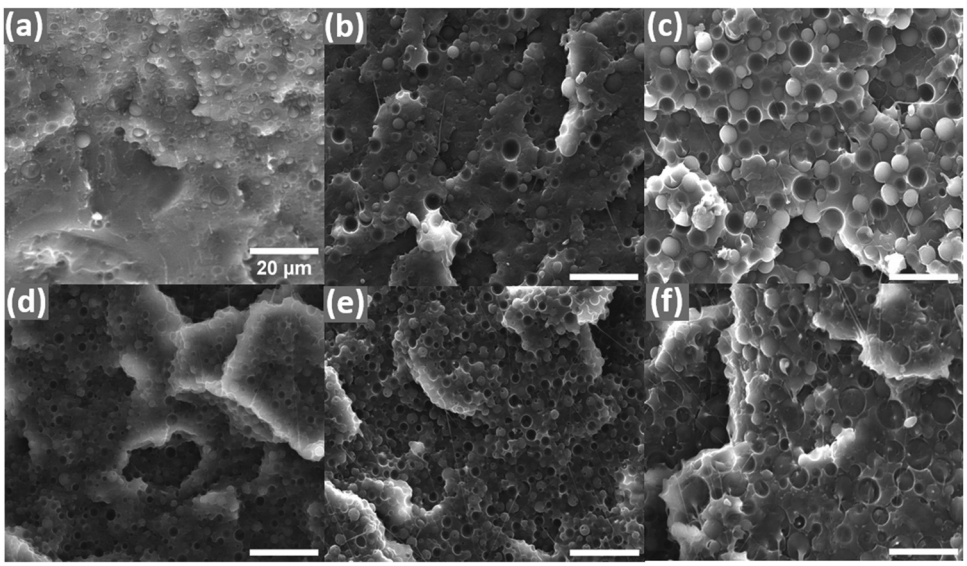

Fig. 2 SEM micrographs of fractured surfaces of PLA/PBAT ((a) 80/20, (b) 70/30, and (c) 60/40) and PLA/PBAT/ECO ((d) 80/20/5, (e) 70/30/5, and (f) 60/40/5) blends. All scale bars are 20 μm.

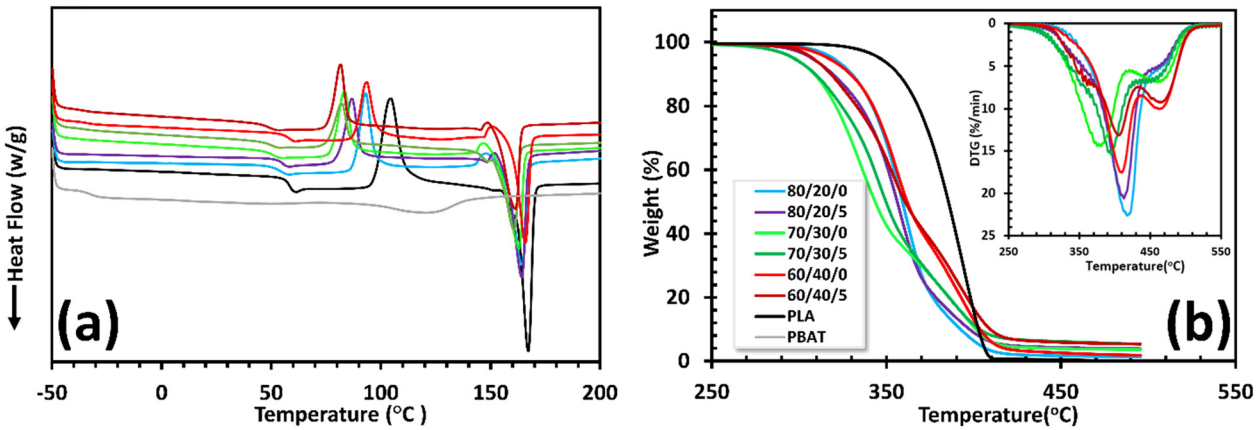

Fig. 3 (a) DSC second heating thermograms and (b) TGA and DTG (inset) curves of pure PLA, pure PBAT, and their blends.

temperature T_{cc} and melting temperature T_m of PLA. More importantly, the crystallization peaks of PLA became sharper upon the addition of ECO, as shown in Fig. S1 (ESI†), which indicates the facilitation of the crystallization. This result is supported by a significant increase in the crystallinity of PLA in the presence of ECO; for instance, it changed from 5.8 to 17.2% for the 80/20 blends with and without ECO, respectively.

The thermal stability of both PLA/PBAT and PLA/PBAT/ECO blends was evaluated by means of thermogravimetric analysis (TGA). This information is important, due to the prolonged exposure to high temperatures experienced by the materials during MEX. Fig. 3b shows the TGA and DTG curves, while Table S3 (ESI†) summarizes the thermal degradation parameters such as the initial weight-loss temperature $T_{5\%}$, which corresponds to the temperature at which a 5% weight loss takes place, T_{max}, which indicates the temperature at which the maximum degradation rate occurs.

According to the DTG curves in Fig. 3b, all PLA/PBAT blends with or without ECO exhibit a two-step degradation behavior, with the first degradation for PLA indicated by T_{max1} and the second one for PBAT represented by T_{max2}. TGA results show that the incorporation of ECO decreases the initial degradation temperature ($T_{5\%}$) for blends with 20 and 40 wt% PBAT, and significantly decreases the T_{max1} of PLA. However, DTG curves showed that the T_{max2} remains constant for all blends with or without ECO.

To further investigate the thermal stability of these blends, isothermal TGA was conducted for both the 70/30/0 and 70/30/5 blends at 190 °C to evaluate the degree of thermal degradation as a function of time (25 min). Fig. S2 (ESI†) confirms that these blends are thermally stable, and the isothermal degradation of these blends at 190 °C was less than 0.3%.

3.4 Rheology

Dynamic oscillatory measurements were performed on PLA/PBAT blends and compatibilized PLA/PBAT/ECO blends to investigate the influence of the blend component concentration and ECO compatibilizer on the blends' rheological properties at 190 °C, which is both the compounding and the MEX processing temperature. In this work, an injection molding grade PLA was chosen, to ensure good flowability during MEX. Fig. 4 illustrates the effect of PBAT concentration on the complex viscosity and storage modulus of PLA. PBAT has higher viscosity, which could make its processing by MEX challenging. Adding PLA is expected to lower the viscosity of the blend, and thus improve its processability. The results showed that

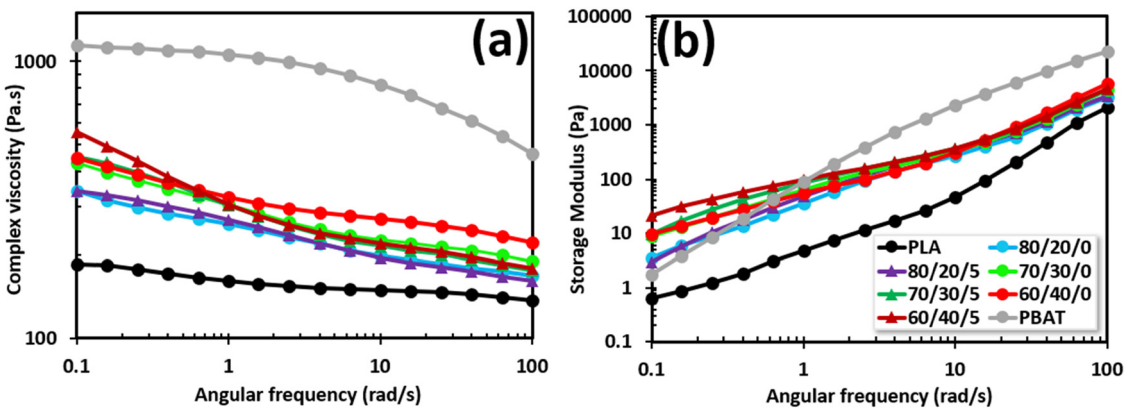

Fig. 4 Rheological properties of PLA/PBAT and PLA/PBAT/ECO blends at 190 °C. (a) Complex viscosity and (b) storage modulus as a function of angular frequency.

higher PLA concentration indeed led to lower complex viscosity and storage modulus, which should facilitate the processing of these blends. The pronounced deviation from the terminal flow of the blends, is attributed to the relaxation of the dispersed PBAT domains.[8,12]

The effect of ECO on the complex viscosity and storage modulus of the compatibilized blends is demonstrated in Fig. 4a and b, respectively. The addition of ECO did not lead to a significant change in the rheological properties of the PLA/PBAT/ECO blends, at all compositions. This suggests that chain-extending or other branching reactions do not occur in the presence of ECO. This strategy is desirable in preparing compatibilized blends for 3D printing applications, because it avoids significant increases in viscosity, which could hinder material extrusion during the printing process. For instance, Joncryl®, an effective compatibilizer for polyester blends, induces branching between PLA and PBAT, resulting in increased viscosities and necessitating higher processing temperatures. Andrzejewski *et al.* found that PLA/PBAT blends compatibilized with Joncryl® are only extrudable above 270 °C, risking degradation of PLA.[20]

3.5 Mechanical properties

The mechanical properties of all the blends are presented in Fig. 5, with Table 2 summarizing the impact strength, tensile modulus, and elongation at break of both compatibilized and non-compatibilized PLA/PBAT blends. As expected, incorporation of the softer PBAT phase reduced the modulus (Fig. 5a). The addition of ECO to PLA/PBAT did not significantly affect the tensile modulus for all blend compositions.

Incorporation of PBAT resulted in improvements in the elongation at break and the impact strength of the blends, compared to neat PLA, but the blends still showed low ductility and toughness. The low toughness of the PLA/PBAT blends is consistent with the morphology analysis, which reveals poor compatibility and weak interface adhesion between the PLA and PBAT phases as the cause of the observed behavior. The incorporation of ECO in the PLA/PBAT blends significantly improved the impact strength for all compositions (Fig. 5c). For instance, the addition of 5 phr of ECO increased the impact strength by 62% and 106% for the blends containing 20 and 30 wt% PBAT, respectively. However, after reaching a concentration of 30 wt% PBAT, there is no further improvement observed in the impact strength.

The addition of ECO to PLA/PBAT blends also significantly improved the elongation at break for all PLA/PBAT/ECO blend compositions (Fig. 5b). For instance, the elongation at break of PLA/PBAT (80/20/0) was only 6.5 ± 0.6%, but when adding a small amount of ECO (5 phr), the elongation at break increased to 27.6 ± 2.4% for the blend (80/20/5).

3.6 MEX 3D printing

Based on the results outlined above, the blend compositions containing 30 wt% PBAT were chosen for the MEX experiments, since they had the best impact properties. As discussed in Section 3.2, increasing the amount of PBAT to 40 wt% resulted in a coarser morphology, and did not produce any improvements in terms of toughness. Fig. 6 compares the tensile stress–strain curves of PLA/PBAT 70/30 and PLA/PBAT/ECO 70/30/5 blends

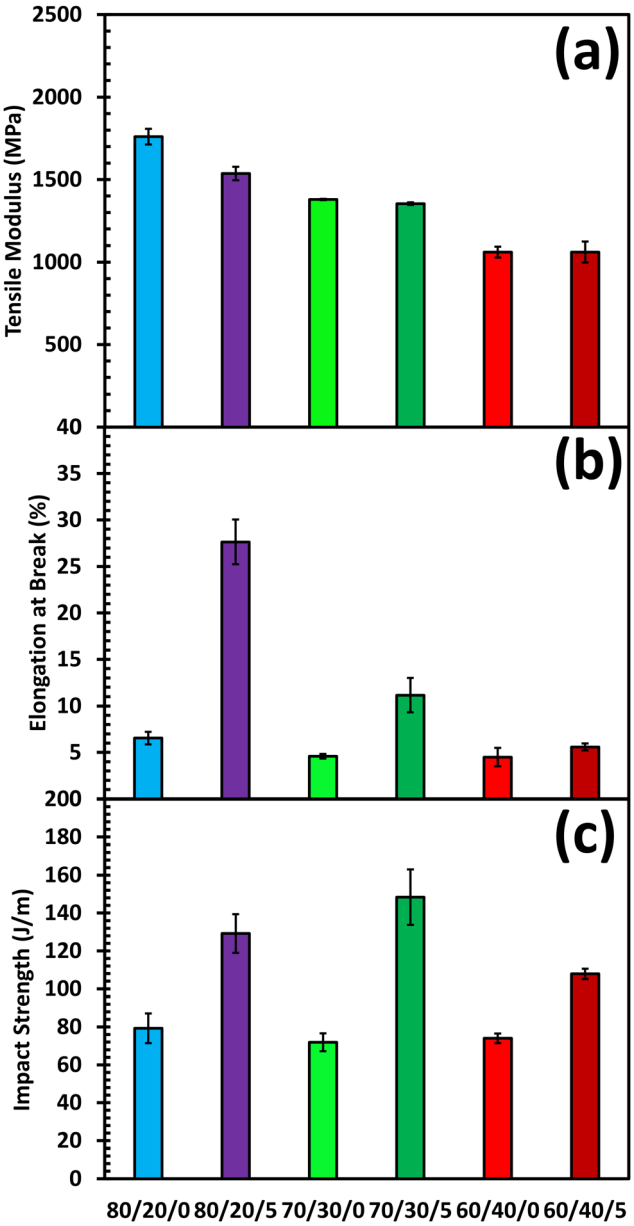

Fig. 5 Effect of ECO on the elongation at break (a), tensile modulus (b), and (c) the impact strength of PLA/PBAT blends.

Table 2 Mechanical properties of PLA/PBAT and PLA/PBAT/ECO blends

PLA/PBAT/ECO	Impact strength (J m^{-1})	Tensile modulus (MPa)	Elongation at break (%)
100/0/0	35.1 ± 0.8	2815 ± 20	2.35 ± 0.4
80/20/0	79.3 ± 7.8	1760 ± 47	6.5 ± 0.6
80/20/5	129.1 ± 10.2	1537 ± 40	27.6 ± 2.4
70/30/0	71.9 ± 4.6	1379 ± 4	4.5 ± 0.2
70/30/5	148.4 ± 14.6	1353 ± 7	11.1 ± 1.8
60/40/0	74.0 ± 2.5	1061 ± 33	4.4 ± 1.1
60/40/5	107.8 ± 2.6	1062 ± 63	5.5 ± 0.3

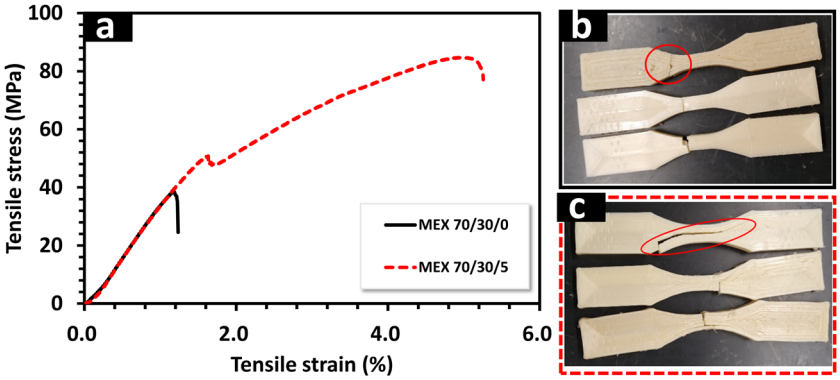

Fig. 6 Stress–strain curves (a) of MEX 3D printed samples of 70/30/0 and 70/30/5 along with fractured tensile specimens ((b) 70/30/0; (c) 70/30/5).

prepared by MEX 3D printing. It is important to note that the existing ASTM or ISO standards are inadequate for testing 3D printed parts, as they fail to account for the lack of integrity attributed to the presence of voids caused by the layering process, the strand deposition pattern, as well as the poor adhesion between the deposited strands.[33–35] Another issue with dumbbell-shaped 3D specimens fabricated by MEX is that they tend to fail outside the gauge section, which is a critical condition for a valid tensile test. Given these limitations, we present the tensile stress–strain curves; albeit we do not report the modulus, tensile stress, and elongation at break because of the above-described inconsistencies involved in these measurements.

The stress–strain curves in Fig. 6(a) show that adding ECO to the PLA/PBAT blends improved the ductility of the printed specimens. Notably, the 3D printed blend containing ECO compatibilizer exhibits a higher tensile stress at break compared to the non-compatibilized PLA/PBAT blend. Similarly, the tensile strain at break was significantly higher for the ECO compatibilized blends. As shown in Fig. 6(b), the PLA/PBAT blend specimens are brittle and exhibit clean fractures, with cohesive failure between the strands, sometimes with failure occurring outside the narrow-gauge section, as indicated by the red circle. On the other hand, the more ductile PLA/PBAT/ECO blends display predominantly adhesive failure, as depicted in Fig. 6c. The failure initiates partially at the narrow section and then continues vertically along the length of the specimen. Overall, 3D-printed specimens with a compatibilized PLA/PBAT/ECO blend demonstrated more consistent and improved mechanical properties. We postulate that this is due to enhanced fusion and minimized voids between the printed strands, which may be due to enhanced diffusion of polymer chains between adjacent strands in the presence of ECO, enabling improved strand healing.[36]

The effect of ECO compatibilizer on interlayer adhesion and diffusion of PLA/PBAT strands during the MEX process can be better seen by examining the SEM images, which showcase the layer-by-layer structure of MEX-printed samples (Fig. 7). Fig. 7(a) reveals a clean brittle fractured surface confirming the low ductility of this blend in the absence of a compatibilizer. Furthermore, the PLA/PBAT blend strands maintain a mostly cylindrical shape, with poor fusion between the strands, resulting in voids.

By incorporating ECO into the PLA/PBAT blend, the morphology and shape of the printed strands improved significantly. Fig. 7(b) reveals a fibrous morphology for a compatibilized blend in the presence of ECO, indicating improved ductility, consistent with the results presented in Section 3.5. Moreover, the printed strands of the compatibilized PLA/PBAT/ECO blend adopt a more rectangular shape. This may be due to the depression of the T_g in the presence of ECO (see Table 1), which allows the polymer to remain in the melt state for a longer time during the cooling process. These enhancements led to a considerable reduction in void size, and improved fusion between the MEX deposited strands, as depicted in Fig. 7(b). Given that interlayer adhesion and void size between layers are crucial parameters governing the mechanical performance of MEX fabricated parts,[36,37] these improvements result in more consistent tensile properties of the printed parts, as discussed in Fig. 6.

These results imply that in addition to the compatibilization effect that we demonstrated earlier, ECO enhances printability and interlayer diffusion. To further investigate this effect, we compared dumbbell specimens printed out of neat PLA and PLA containing 5 phr ECO. SEM micrographs in Fig. S3 (ESI†) show the cross-sectional alongside the top surface of the neat PLA and PLA/ECO samples. Fig. S3(b) (ESI†) shows that ECO effectively improved the interstrand diffusion compared to the neat PLA (Fig. S3(a), ESI†), leading to improved healing between the neighboring strands. Furthermore, blending ECO with PLA

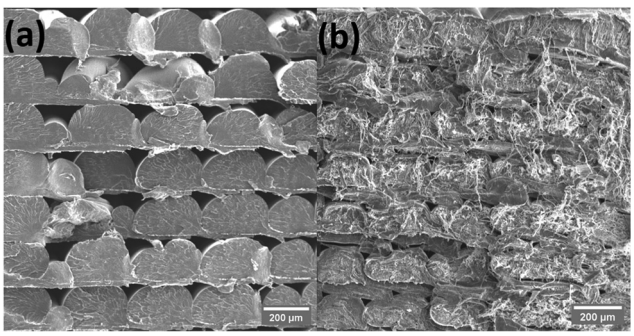

Fig. 7 SEM images of fractured cross-sectional surfaces of MEX printed tensile specimens of PLA/PBAT ((a) 70/30/0) and PLA/PBAT/ECO ((b) 70/30/5).

also led to a significant reduction in the size of the air voids within printed strands as shown in Fig. S3(c and d) (ESI†). Given that ECO did not significantly alter the rheological and thermal properties of the polymers, we postulate that the low molecular weight oil migrates during extrusion, thus coating the strands and acting as a processing aid. The epoxy functional groups of the ECO might further engage in complex interactions, thus improving interdiffusion and facilitating bonding between neighboring strands, resulting in a substantial reduction in void size between the strands.[36,38]

4. Conclusions

In this study, we investigated the compatibilizing effect of ECO on PLA/PBAT blends, aiming at developing formulations that are suitable for MEX-3D printing. The incorporation of ECO into the PLA/PBAT blends resulted in significant improvements in the compatibility between these polymers, leading to well-dispersed and uniform PBAT domains within the PLA matrix. The enhanced compatibility between PLA and PBAT in the presence of ECO resulted in a 62% and 106% increase in impact strength for blends containing 20 and 30 wt% PBAT, respectively, compared to non-compatibilized blends. Rheological analysis indicated that the viscosity of the PLA/PBAT blends can be adjusted to make them suitable for MEX 3D printing, while addition of ECO did not result in significant changes in the rheological properties, or the thermal stability of the blends. DSC measurements revealed a plasticizing effect in the presence of ECO, resulting in a suppression of the T_g and cold crystallization temperatures. The 70/30 PLA/PBAT blend with 5 phr ECO, which exhibited optimal impact strength, was selected, and subjected to MEX printing. Dumbbell specimens printed from non-compatibilized PLA/PBAT blends displayed poor fusion between the strands, resulting in larger voids that caused brittle failure during tensile testing. The addition of ECO facilitated fusion between neighboring strands and reduced the number and size of air voids between deposited strands, resulting in a significant enhancement in interlayer adhesion and tensile ductility. These findings highlight the potential use of ECO as an environmentally friendly compatibilizer and processing aid to enhance the 3D printing capabilities of PLA/PBAT blends, offering improved mechanical performance, better interlayer healing, fewer interlayer voids, and overall higher print quality. This will pave the way to transforming PLA from being merely a material choice for prototyping and 3D printing hobbyists to being suitable for use in specialty end-use parts, such as devices, components for aerial vehicles, telecommunications, *etc.*

Conflicts of interest

There are no conflicts to declare.

References

1 E. F. Fiandra, L. Shaw, M. Starck, C. J. McGurk and C. S. Mahon, *Chem. Soc. Rev.*, 2023, **52**, 8085–8105.
2 S. Su, R. Kopitzky, S. Tolga and S. Kabasci, *Polymers*, 2019, **11**, 1193.
3 M.-O. Augé, D. Roncucci, S. Bourbigot, F. Bonnet, S. Gaan and G. Fontaine, *Eur. Polym. J.*, 2023, **184**, 111727.
4 V. Ojijo, S. S. Ray and R. Sadiku, *ACS Appl. Mater. Interfaces*, 2013, **5**, 4266–4276.
5 L. Song, Y. Li, X. Meng, T. Wang, Y. Shi, Y. Wang, S. Shi and L. Z. Liu, *Polymers*, 2021, **13**, 3245.
6 G. Spinelli, P. Lamberti, V. Tucci, R. Kotsilkova, E. Ivanov, D. Menseidov, C. Naddeo, V. Romano, L. Guadagno, R. Adami, D. Meisak, D. Bychanok and P. Kuzhir, *Materials*, 2019, **12**, 2369.
7 A. Z. Naser, I. Deiab, F. Defersha and S. Yang, *Polymers*, 2021, **13**, 4271.
8 M. Bianchi, A. Dorigato, M. Morreale and A. Pegoretti, *Polymers*, 2023, **15**, 881.
9 S. Nikolov, M. Petrov, L. Lymperakis, M. Friak, C. Sachs, H. O. Fabritius, D. Raabe and J. Neugebauer, *Adv. Mater.*, 2010, **22**, 519–526.
10 M. Nerkar, J. A. Ramsay, B. A. Ramsay, A. A. Vasileiou and M. Kontopoulou, *Polymer*, 2015, **64**, 51–61.
11 J. Sempere-Torregrosa, J. M. Ferri, H. de la Rosa-Ramirez, C. Pavon and M. D. Samper, *Polymers*, 2022, **14**, 4205.
12 X. Wang, S. Peng, H. Chen, X. Yu and X. Zhao, *Composites, Part B*, 2019, **173**, 107028.
13 R. Al-Itry, K. Lamnawar and A. Maazouz, *Polym. Degrad. Stab.*, 2012, **97**, 1898–1914.
14 D. Wu, A. Huang, J. Fan, R. Xu, P. Liu, G. Li and S. Yang, *J. Polym. Eng.*, 2021, **41**, 95–108.
15 J. Jian, Z. Xiangbin and H. Xianbo, *Adv. Ind. Eng. Polym. Res.*, 2020, **3**, 19–26.
16 H.-T. Chiu, S.-Y. Huang, Y.-F. Chen, M.-T. Kuo, T.-Y. Chiang, C.-Y. Chang and Y.-H. Wang, *Int. J. Polym. Sci.*, 2013, **2013**, 1–11.
17 Y. Han, J. Shi, L. Mao, Z. Wang and L. Zhang, *Ind. Eng. Chem. Res.*, 2020, **59**, 21779–21790.
18 J. Chen, C. Rong, T. Lin, Y. Chen, J. Wu, J. You, H. Wang and Y. Li, *Macromolecules*, 2021, **54**, 2852–2861.
19 Y. Deng, C. Yu, P. Wongwiwattana and N. L. Thomas, *J. Polym. Environ.*, 2018, **26**, 3802–3816.
20 J. Andrzejewski, J. Cheng, A. Anstey, A. K. Mohanty and M. Misra, *ACS Sustainable Chem. Eng.*, 2020, **8**, 6576–6589.
21 J. S. Jeon, D. H. Han and B. Y. Shin, *Adv. Mater. Sci. Eng.*, 2018, **2018**, 1–8.
22 P. Ma, X. Cai, Y. Zhang, S. Wang, W. Dong, M. Chen and P. J. Lemstra, *Polym. Degrad. Stab.*, 2014, **102**, 145–151.
23 Q. Litke, M. Wahbi, M. Kontopoulou, D. B. Levin and S. Liu, *J. Mater. Sci.*, 2023, **58**, 17691–17710.
24 S. Qiu, Y. Zhou, G. I. N. Waterhouse, R. Gong, J. Xie, K. Zhang and J. Xu, *Food Chem.*, 2021, **334**, 127487.
25 N. T. Kilic, B. N. Can, M. Kodal and G. Ozkoc, *J. Appl. Polym. Sci.*, 2018, **136**, 47217.
26 J. Mathew, J. P. Das, M. Tp and S. Kumar, *J. Polym. Res.*, 2022, **29**, 474.
27 Y. Lyu, Y. Chen, Z. Lin, J. Zhang and X. Shi, *Compos. Sci. Technol.*, 2020, **200**, 108399.

28 M. Bailly and M. Kontopoulou, *Polymer*, 2009, **50**, 2472–2480.
29 M. P. W. Long Jiang and J. Zhang, *Biomacromolecules*, 2006, **7**, 199–207.
30 E. Jalali Dil, P. J. Carreau and B. D. Favis, *Polymer*, 2015, **68**, 202–212.
31 J. Gonzalez Ausejo, J. Rydz, M. Musioł, W. Sikorska, M. Sobota, J. Włodarczyk, G. Adamus, H. Janeczek, I. Kwiecień, A. Hercog, B. Johnston, H. R. Khan, V. Kannappan, K. R. Jones, M. R. Morris, G. Jiang, I. Radecka and M. Kowalczuk, *Polym. Degrad. Stab.*, 2018, **152**, 191–207.
32 A. Lopera-Valle, J. V. Caputo, R. Leao, D. Sauvageau, S. M. Luz and A. Elias, *Polymers*, 2019, **11**, 933.
33 A. R. Torrado and D. A. Roberson, *J. Fail. Anal. Prev.*, 2016, **16**, 154–164.
34 S. A. Tronvoll, T. Welo and C. W. Elverum, *Int. J. Adv. Manuf. Technol.*, 2018, **97**, 3607–3618.
35 A. Sola, W. J. Chong, D. Pejak Simunec, Y. Li, A. Trinchi, I. Kyratzis and C. Wen, *Polym. Test.*, 2023, **117**, 107859.
36 Y. S. Ko, D. Herrmann, O. Tolar, W. J. Elspass and C. Brändli, *Addit. Manuf.*, 2019, **29**, 100815.
37 D. Lee and G. Y. Wu, *Polymers*, 2020, **12**, 2456.
38 W. Prasong, A. Ishigami, S. Thumsorn, T. Kurose and H. Ito, *Polymers*, 2021, **13**, 740.